JOURNAL OF CATALYSIS 148, 288–303 (1994)

Modeling the Thiophene HDS Reaction on a Molecular Level

E. Diemann, Th. Weber,* and A. Müller

Faculty of Chemistry, University of Bielefeld, P.O. Box 100131, 33501 Bielefeld, Germany

Received March 8, 1993; revised August 2, 1993

The structure of MoS_2/Al_2O_3 catalyst and the initial step of the hydrodesulfurization (HDS) reaction using an *experimental* model have been studied by *in situ* Raman-, infrared emission (IRE)-, inelastic electron tunneling (IET)-spectroscopy and thermal desorption measurements accompanied by molecular modeling and EH-MO calculations. The results show that the catalyst consists of MoS_2-like crystallites which are linked via Mo–O–Al bonds [*d*(Mo–O) ca. 185 pm, angle Mo–O–Al ca. 140°] almost perpendicular (but slightly inclined) to the surface of γ-Al_2O_3. A pretreatment of the surface of the MoS_2 crystallites with hydrogen is mandatory to remove all kinds of S_2 groups and to form active (formally) Mo^{II} centers at the edge positions. Thiophene, acting as a Lewis acid *only* towards such centers, is destabilized upon coordination and becomes susceptible for further reaction with hydrogen which may follow, in principle, within the first steps of the route of a Birch reduction.

INTRODUCTION

The optimization of large scale industrial processes with respect to economic and environmental problems is an interdisciplinary research subject of fundamental significance. One of the most important procedures employed worldwide is the refining of crude oils which involves catalytic hydrodesulfurization (HDS), hydrodenitrogenation (HDN), hydrodeoxygenation (HDO), and hydrodemetallation (HDM). Although these reactions have already been used successfully over many years, the structure of the catalysts as well as the underlying reaction mechanisms are still controversial. During the HDS reaction sulfur-containing molecules are converted at medium high pressures of H_2 and ca. 670 K into hydrogenated compounds and H_2S typically employing a $CoMoS/Al_2O_3$ catalyst. The extreme reaction conditions are often outside the scope of many measuring techniques. Furthermore, the noncrystalline character of the catalyst hinders an accurate X-ray structure determination and the many adjustable parameters during the preparation of the catalyst and during the course of the reaction itself are the main reasons why many of the reported results are not really comparable. This contributes to the numerous contradictions found in the literature. Recent compilations of the state of research may be found in Refs. (1) and (2).

To try for a new systematic approach towards the solution of this problem we have selected considerably-simplified *experimental* model systems which have the advantage over many others that much unequivocal structural and spectroscopic information is available for the compound chosen as catalyst precursor and its chemical reactions (3, 4). The chosen precursor also shows reasonable HDS activity for thiophene as the usually employed model organic reactant. Our system starts from $(NH_4)_2[Mo_3S_{13}] \cdot H_2O$ as a precursor for which the thermal decomposition has been studied in some detail (4) and where the model character of the corresponding anion (I) for the surface of MoS_2 has been illustrated instructively (5).

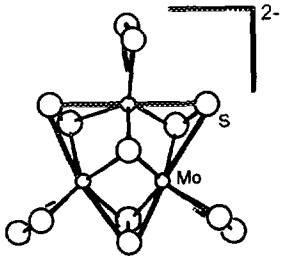

(I)

The preparation of catalysts from this precursor and their activity has already been reported (6). The introduction of *promoters* (such as Co or Ni) and *modifiers* (such as P or F) atoms will be reserved for a later step in this approach.

To characterize the precursor and the catalyst with and without loading we have used three different experimental techniques. The first one, *in situ* Raman spectroscopy, has already been shown to be a particularly powerful tool for these kinds of studies (7, 8). The other two, i.e., infrared emission spectroscopy (IRE) (9) and inelastic

* Present address: Schuit Institute of Catalysis, Technical University of Eindhoven, P.O. Box 513, 5600 MB Eindhoven, The Netherlands.

0021-9517/94 $6.00

electron tunneling spectroscopy (IET) (10–12) are much less widespread and some features of these techniques merit recall.

IRE has the advantage over many other forms of spectroscopy in that *in situ* measurements of surface species are possible without treating the sample with any kind of electromagnetic radiation. Only the emission from the heated sample is collected, where mainly the surface contributes to the measuring result.

IET is a nonoptical vibrational spectroscopy of high sensitivity which has reasonable resolution (at cryogenic temperatures), is free of the normal optical selection rules and is applicable to the study of thin film oxides (e.g., Al_2O_3 on Al) and also adsorbates on them down to a monolayer coverage of approximately 2%; however, no commercial spectrometer is available. It has been successfully applied to some topics of surface chemistry, viz. adhesion and trace impurity detection, surface and solid state physics, and, essentially, to the study of metal-molecule interactions (10). We found that the difficulties involved in designing a complete and properly working setup were more than compensated by the advantage of obtaining new insights into the bonding and orientation of the slabs on the support and of the organic reactant (here referred to as the substrate) adsorbed on the crystallites. A particularly strong point in favour of this method is the functional relationship between the relative orientation of the vibrating units and the intensities of the corresponding signals observed in the spectra ("orientation selection rules"). Although the measurements must be done at cryogenic temperatures (4.2 K, liquid He), the spectral results correspond to the structural situation of the catalyst at about 470 K as a consequence of the specific sample preparation procedure (see below).

IET has been used for the study of molecular adsorbates (organic substrates) on metal oxides in more than 300 papers (11), but only a small minority of them deal with inorganic clusters and metal particles supported on alumina with a view to problems of heterogeneous catalysis (12). The subsequent preparation of an IET sample including all features of an HDS catalyst under working conditions (support, catalyst, substrate) is attempted here for the first time.

At a later step of our studies, to clarify the conditions for the chemisorption of thiophene at the active sites of our model system, we had to introduce the additional well-known technique of temperature programmed desorption (TPD) (13).

All measurements were accomplished with the same or at least a similar system. Moreover, the system under study could be determined with such a degree of reliability that a direct comparison with results from theoretical approaches, i.e., molecular modeling and Extended Hückel calculations, became possible.

METHODS AND MATERIALS

$(NH_4)_2[Mo_3S_{13}] \cdot H_2O$ was used throughout as starting material for the preparation of the MoS_2 crystallites (5). It can easily be prepared in almost quantitative yield by the reaction of an aqueous solution of ammonium heptamolybdate with hot ammonium polysulfide solution (14). As support we used a commercial ultrapure alumina (EC 413 from Pro Catalyse, surface area 238 m^2/g). The catalyst precursor was prepared by the "dry impregnation" of the support with the molybdenum cluster compound (6). Typically, 2 g Al_2O_3 were impregnated for 2 h with a solution of 564 mg $(NH_4)_2[Mo_3S_{13}] \cdot H_2O$ in 3 ml *N,N*-dimethylformamide. The solvent was evaporated in vacuum and the sample stored in a sealed bottle under argon. Prior to use the precursor was heated to 670 K for 16 h in an Ar atmosphere for each experiment. Thiophene (Merck 808157) was used after distillation as a standard substrate for the catalyzed reaction. Hydrogen (Linde 4.5), argon (Linde 4.0) and hydrogen sulfide (Gerling-Holz 4.0) were taken direct from high pressure cylinders.

Macrocrystalline MoS_2 was used as supplied from Alfa Chemicals. It is usually obtained by the method of Van Arkel (15), i.e., heating stoichiometric amounts of the elements in an inert atmosphere. Amorphous or microcrystalline MoS_2 was prepared *in situ* in the emission cell by sulfiding MoO_3 with 10% H_2S/H_2 for 4 h at 670 K or by thermal decomposition of the cluster compound $(NH_4)_2[Mo_3S_{13}] \cdot H_2O$ as described above, respectively.

In Situ Raman Spectroscopy

The Raman setup including a detailed description of our *in situ* cell has been reported previously (8). The Raman spectra were recorded using a Spex Ramalog V (triple monochromator) and a Coherent Innova 70/4 Ar^+ laser. The 514.5-nm line was employed with an incident power of 100 mW. Spectra accumulation and data processing were done using a self-designed program run on a microcomputer, which was connected to the monochromator unit. The powdered precursor was pressed into an 11 mm diameter self-supporting disk and mounted on the sample holder of the *in situ* cell. The apparatus was purged with argon and in the case of the catalyst pretreatment heating was carried out as described above. For coordinating the substrate the sample was loaded with H_2/thiophene (saturated at 273 K, flow rate 50 ml/min) at 670 K for 2 h and the Raman spectrum was recorded under these conditions.

Infrared Emission Studies

The theoretical and instrumental aspects of this method (16) and different kinds of IRE cells (17, 18) are described in the literature. Our design is depicted in Fig. 1. It allows

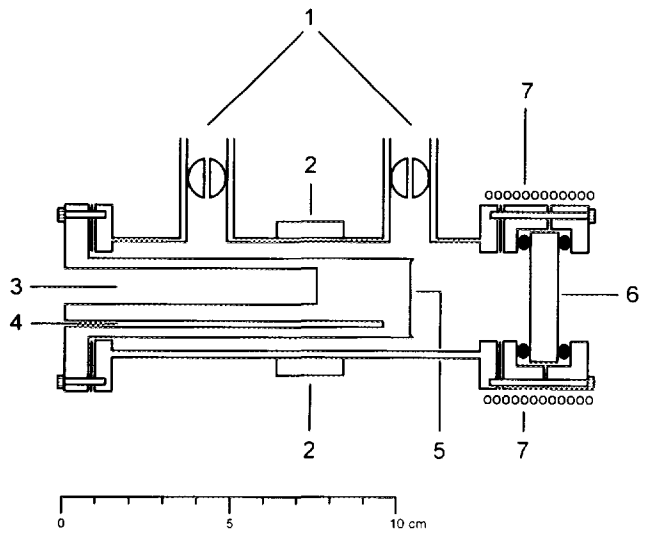

FIG. 1. Infrared emission cell (schematic); for explanation, see text.

"sample activation" up to 770 K in vacuum or controlled atmospheres. It consists of three parts, made of stainless steel and sealed by annealed copper gaskets in the high temperature area. The central part, a cylindrical tube of 4 cm in diameter, includes joining flanges for the furnace (on the left) and the window-unit (on the right), inlets with ball valves (1) for evacuation and gassing, as well as a clamp (2) connected to a positioning mechanism for fine adjustment of the cell in the spectrometer. The furnace unit is heated via a 250 W resistor heater block (to simplify the design we used a 250 W soldering ion with a modified copper tip). This heater block was inserted into hole (3) and regulated via the response of a thermocouple inserted in hole (4). The CsI window (6) is sealed with Viton O-rings and kept at room temperature by water cooling (7). The temperature fluctuation measured at the end of the furnace (polished plate; sample deposit (5)) is only about 1 K due to the thermal inertia of this part. A constant cell temperature is important to achieve high quality emission spectra, because the energy amount emitted by the sample depends principally on the temperature (as given by the Stefan–Boltzmann law). In practice, artifacts such as weak bands or shoulders can be observed due to variations of the same temperature (19).

In principle, the infrared source of the spectrometer has only to be replaced by the emission cell. Our measurements were made with a Mattson Polaris FTIR spectrometer employing a CsI beamsplitter and a DTGS pyroelectric detector. With this instrument the modification for the emission measurements is particularly easy, because only one mirror has to be substituted by the emission cell. The spectral resolution for our studies was typically 8 cm^{-1}. Each spectrum is the sum of 500 scans vs the ("black body") emission of the cell without sample. The raw data set was transmitted to a microcomputer, where further processing was done with a self-designed program package which also includes algorithms for baseline correction and data smoothing. However, for the results reported here no such kind of data handling was necessary; therefore, each spectrum represents the genuine result of the measurement. The apparatus was purged with argon and heated to 670 K, which took about 4 min employing maximum power.

Besides a constant cell temperature, the preparation of the sample as a homogeneous thin layer on the furnace of the cell (19) is essential for spectra of acceptable quality. This was achieved by shaking 1 mg of the sample and 5 ml of 2-propanol for 10 min in a vibrating mill. The resulting suspension was spread on the furnace area of the emission cell and the liquid was slowly evaporated. The distribution of the resulting layer was typically $\approx$0.2 mg/cm^2, which gives an average thickness of $\approx$0.5 μm. The spectra of the macrocrystalline MoS_2 were measured after thermal equilibration, and those of the amorphous MoS_2 compounds after completing the preparation procedures (see above) and at given time steps. The spectrum of the adsorbed substrate was obtained in argon after loading the catalyst for 2 h with H_2/thiophene (see above). Regardless of the specific preparation or pretreatment conditions, all emission spectra in this paper were recorded at 670 K in an Ar atmosphere.

Inelastic Electron Tunneling Spectroscopy

The theory and technique together with a description of the experimental setup are given in Ref. (20). Our measuring circuit is displayed in Fig. 2((a), function diagram; (b), circuit diagram) and also includes several points of optimization as discussed by Walmsley *et al.* (21). It is composed of seven independent units (Fig. 2a), namely the ramp generator, a function generator including additional filter elements, the sample (tunnel junction), a frequency selective 2ω transformer amplifier and the detection unit (preamplifier and lock-in amplifier with an x–y recorder). The ramp generator (see Fig. 2b) consists of a 24 V battery and a motor-driven potentiometer employing a sweep from 0 to 24 V. The actual energy range, typically 20–200 meV (corresponding to 160–1600 cm^{-1}; 1 meV $\equiv$ 8.065 cm^{-1}) is obtained via a potential division circuit including the sample as resistor. A modulation voltage (ω = 50 kHz, U_{mod}^{p-p} = 1.8 mV) is added to the ramp using a Philips PM5217 function generator with an additional serial 2ω and parallel ω filter element. Due to tunneling phenomena across the junction a signal at 2ω is generated, which is then transformed and (2ω) selectively amplified. As detection circuit a preamplifier (OP TL082) and lock-in amplifier (EG&G Princeton Applied Research, Model

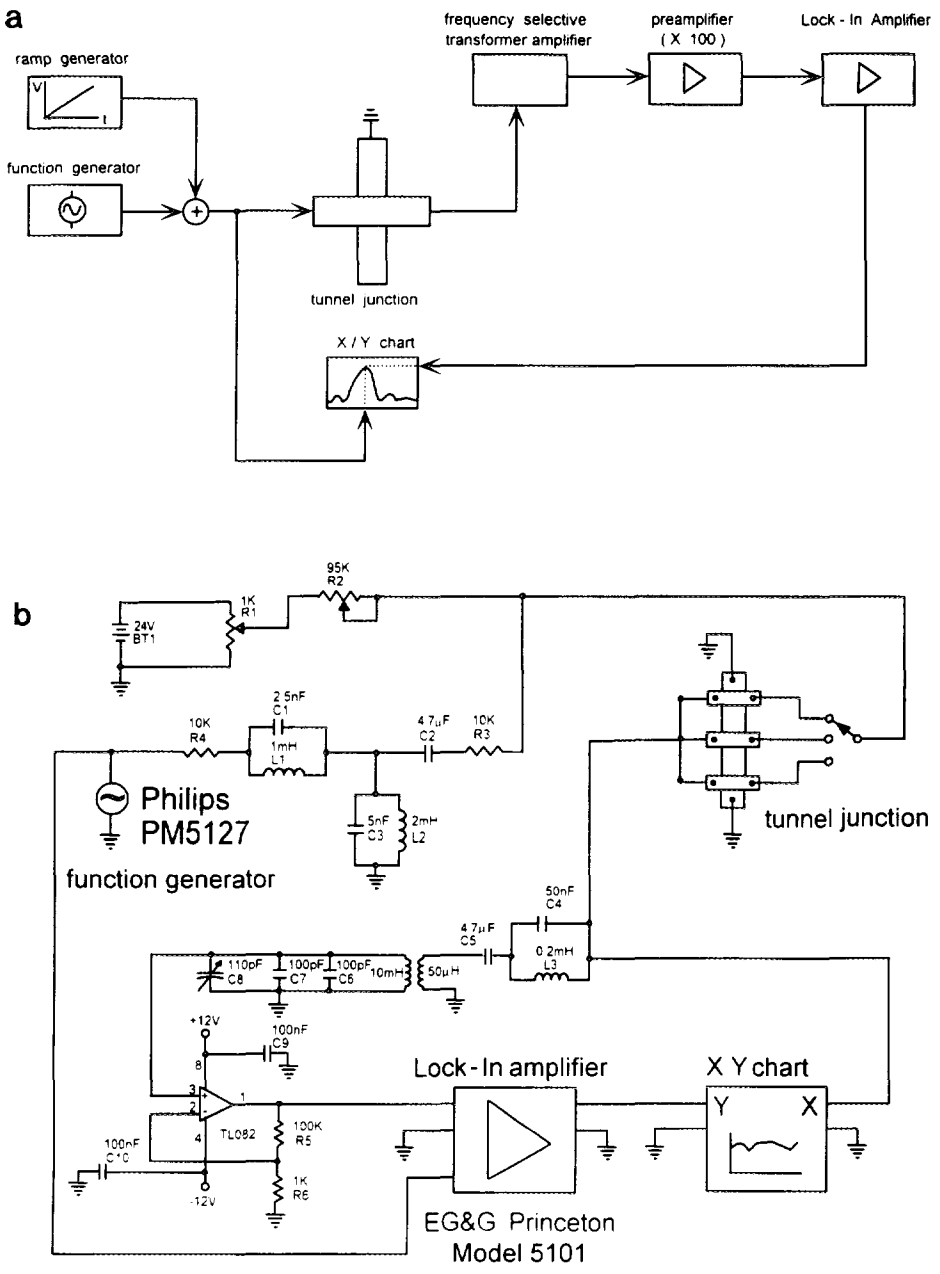

FIG. 2. Block diagram (a) and circuits (b) for the measurement of IET spectra (see text).

5101) connected to an x–y chart recorder (Linseis) was used.

In principle, the system under investigation is prepared as an insulating barrier, separating two metal electrodes, typically Al and Pb, electrically with a resistance between 50 and 500 Ω. Associated with an applied voltage sweep the tunnel current interacts inelastically with the barrier system in simultaneous excitation of all normal modes which have their main displacement parallel to the tunneling direction.

Important points and the general experimental setup for the preparation of the tunneling junctions can be found in the compilation of Tomlin (22). We have used a corresponding self-constructed reaction chamber operated with an oil diffusion pump (Edwards Diffstak System 63/150). An additional controlled-atmosphere high temperature reactor connected to the reaction chamber via an inert atmosphere glove box was used for the preparation of the catalyst samples. Evaporation of Al and Pb (both from Balzers, 99.999%), was achieved using tungsten boats (Balzers) as working resistor for a high current transformer (6 V/300 A).

Glass slides were used as support for every five junctions of 4 mm^2 prepared together. Prior to use the slides were kept for 4 h in a detergent solution in an ultrasonic bath, for one further day in 40% KOH, for a further day in 70% sulfuric acid, rinsed for 30 min with distilled water, and stored under ethanol. To save time we have machined a magazine from Teflon where 24 slides could be cleaned at the same time. Care has to be taken that only absolutely clean and dry slides are mounted in the preparation vessel. The first evaporated layer (at a pressure of 2.6×10^{-3} Pa) was always aluminium with an average thickness of 100 nm. To grow a layer of pin-hole-free alumina two kinds of oxidation procedures were used, namely the oxidation in a current discharge oxygen plasma ($p(O_2) \approx 1.06$ Pa, 4 mA) and a thermally induced (590 K) growth of Al_2O_3 from freshly evaporated Al exposed to clean air and pure oxygen (oxidation by residual oxygen in the lattice). The thickness of the γ-Al_2O_3 layer is typically about 3 nm and determines essentially the resistance of the junction. Doping of this layer with the $[Mo_3S_{13}]^{2-}$ cluster compound was made analogous to the "dry impregnation" procedure (vide supra), i.e. by applying 1 μl of a 10^{-4} *M* solution of the cluster compound in acetonitrile to each effective junction area and subsequently removing the solvent in vacuum. Three types of junctions have been prepared with this starting system:

(i) the counter-electrode was deposited directly (evaporation pressure $\approx 6.6 \cdot 10^{-3}$ Pa),

(ii) the junctions were heated under Ar to 590 K for 5 h, cooled to room temperature and covered with the counter-electrode, and

(iii) the same as (ii), but after heating under Ar the sample was loaded with H_2/thiophene for 2 h at this temperature (see above). After cooling, the physisorbed thiophene was removed in an Ar stream (flushing for 1 h at room temperature) and the counter-electrode was deposited as above.

The Al_2O_3 layer for (i) was prepared by plasma oxidation, for (ii) and (iii) by thermally induced oxidation. During the thermal evaporation and the deposition of the lead counter-electrode the local temperature rises to $\approx$470 K and the system is quenched (matrix captured) in this state. The slides were mounted to a specially designed probe (22, 23), then cooled with liquid nitrogen and subsequently inserted into a liquid helium Dewar vessel. The spectra were recorded throughout at 4.2 K giving a reasonable reduction of the thermal linewidth broadening ($5.4\ kT \approx 15\ cm^{-1}$). The scan speed was 5 mV/min and the lock-in time constant was 3 s for all experiments.

Temperature Programmed Desorption (TPD)

The TPD measurements were performed, in principle, as described in the literature (13). All procedures, i.e. the catalyst pretreatment, activation and loading with thiophene could be done in a closed system; for this study the desorption was detected with a Penning gauge and the connection of the apparatus to a mass spectrometer was not of interest. Three types of samples have been studied:

(i) the precursor heated in Ar, loaded with H_2/thiophene for 2 h and cooled to room temperature in this atmosphere,

(ii) the precursor heated in Ar, loaded with Ar/thiophene for 2 h and cooled to room temperature in this atmosphere, and finally

(iii) the pure Al_2O_3 support under the same conditions as for (i).

The initial pressure was 2.6×10^{-3} Pa (as obtained with an Edwards Diffstak System 63/150 oil diffusion pump) and the heating rate was 10 K/min. Both the desorption volume and the amount of sample were chosen to give typically an increase in the pressure of two orders of magnitude upon desorption of the chemisorbed thiophene. The temperature scale studied ranged from room temperature to 720 K.

MOLECULAR MODELING AND EH-MO CALCULATIONS

Molecular modeling with a digital computer employing force field methods is an already established technique to obtain the "best" geometrical arrangement for a given connectivity of atoms from a set of optimized parameters. Here it is used to obtain information about the relative conformation and space filling of either the support surface with the catalyst particle or the latter with the substrate (cf., e.g., (24)), but only in a semiquantitative way to indicate direction and potentiality. For our calculations we used the MMX force field, as implemented in PCMODEL386 (Vers. 4.0) from Serena Software, Bloomington, IN, USA; the underlying potential functions are those for MM2 (cf. Ref. (25)). The provided parameters gave within an accuracy of 1% the correct geometries for related metal sulfur clusters (like the $Mo_3S_{13}^{2-}$ anion) where the structures are known from crystal structure determinations. Due to restrictions caused either by the available computer memory or the employed minimizing algorithm we could not extend the calculations to a system of the real expected size of the catalyst particle, i.e., ca. 5500 pm. Instead we were forced to model only sections of it but gave them a backbone of fixed distances and artificially high force constants for the bonds forming it. This is a reasonable approximation since here we were concerned only with the geometrical requirements of the interface region and these will very probably not differ too much from the situation in the real system where the surfaces are backed by larger volumes of an ordinary crystal structure

with high bonding or lattice energies. In particular, we were concerned with the following situations:

(i) docking of a thiophene molecule to the free Mo site of an $[Mo_3S_{13}]^{2-}$ cluster anion (structure I) where one of the terminal S_2 groups had been removed,

(iii) docking of thiophene to coordinatively unsaturated Mo edge atoms of a section from the MoS_2 lattice consisting of three layers.

(iii) the same as before, but docking a dibenzothiophene substrate, and finally

(iv) docking small single and triple layer sections with MoS_2 structure to the surface of γ-Al_2O_3.

The model system for our Extended-Hückel MO calculations again was derived from the $[Mo_3S_{13}]^{2-}$ cluster ion, for which also the results of an Xα-SW calculation are available (26). To simulate the first step of the catalytic cycle we have eliminated reductively one neutral S_2 group and docked thiophene to this free site with coordinates as obtained from the molecular modeling. The calculations were done with two different computer programs. For the iterative computations (change iteration on the metal atoms to reach self consistent charge and configuration, SCCC, modified from QCPE 256 cf. Ref. (27)) we used multi-ζ radial functions for molybdenum as reported by Basch and Gray (28) and the single-ζ values for sulfur, carbon, and hydrogen from Clementi (29). The VOIP curves for the charge iteration of Mo were taken from Ref. (30) as for Cr but with reduction of the coefficient C by 1.24 eV as proposed in Ref. (31). The H_{ii} values for sulfur were those for the hydride and were kept constant at -20.7 for S $3s$ and -11.6 eV for S $3p$. For C $2s$ H_{ii} was set to -21.4, for C $2p$ to -11.4 and to -13.6 eV for H $1s$, respectively. The H_{ij} elements were obtained from the Wolfsberg–Helmholz formula (32) using a Hückel constant $k = 1.75$. A second, noniterative EH-MO program (33) was used to prepare the orbital plots utilizing the final parameters of the SCCC calculations.

RESULTS AND DISCUSSION

The IRE (a), Raman (b), and IET (c) spectra of our catalyst precursor, i.e., $(NH_4)_2[Mo_3S_{13}] \cdot H_2O$, ((b) and (c) on alumina, respectively) are displayed in Fig. 3, showing the characteristic bands of the cluster anion. In the IRE and Raman spectra the bands with highest intensity are those due to the ν(S–S) vibrations. According to the different bond lengths in the bridging and the terminal S_2 groups, there are bands at higher ($\nu(S–S)_{br}$ = 553(Raman), 544(IRE) cm^{-1}) and lower wavenumbers ($\nu(S–S)_t$ = 522(Raman), 505(IRE) cm^{-1}). Another characteristic feature of this compound is the ν(Mo–S) vibration of the central ("apical") sulfur (466(Raman), 460(IRE) cm^{-1}). The bands at lower wavenumbers are due to ν(Mo–S)

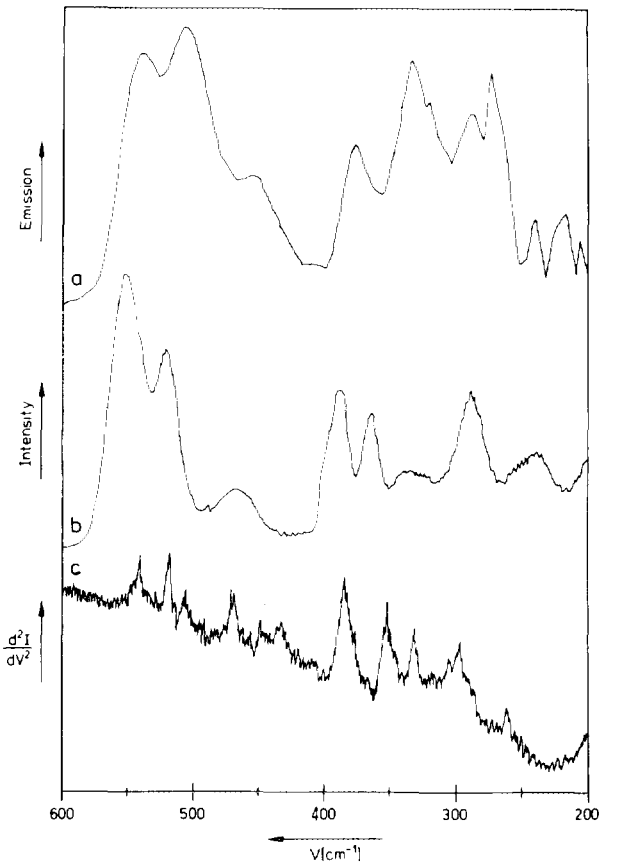

FIG. 3. IRE (a), Raman (b), and IET (c) spectra of $(NH_4)_2[Mo_3S_{13}] \cdot H_2O$ ((a) without support; (b) and (c) on γ-Al_2O_3).

type vibrations in the range of 400–270 cm^{-1} and are not characteristic for the different types of bonds to such an extent. Below 200 cm^{-1} bands are found which correspond to vibrations which contain metal–metal stretching contributions (34). Further details including a proof for these assignments by means of isotope substitution experiments have been reported by Fedin *et al.* (35).

As already mentioned, the intensities I of bands observed in the IET spectrum are closely related to the orientation of the vibrating units relative to the tunneling current. Since $I \sim \cos^2 \theta$ (θ is the angle between the direction of the displacement due to the vibration and the tunneling direction), we expect bands with higher intensities if the displacements of the vibrations are parallel and, correspondingly, with lower intensities if they are perpendicular to the tunneling direction. If a preferred orientation is missing, an average of Raman and IR intensities will be observed. Our IET spectrum (Fig. 3c) implies that the $[Mo_3S_{13}]^{2-}$ cluster anion "stands" via one terminal S_2 group on the alumina surface as depicted schematically in Fig. 4. This kind of orientation follows from the observed relative band intensities: $\nu(S–S)_{br}$ = 540 (*m*); $\nu(S–S)_t$ = 517 (*m*) 506 (*w*); $\nu(\mu_3S–Mo_3)$ = 469 (*m*);

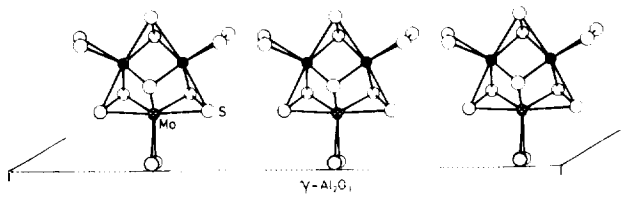

FIG. 4. Orientation of the $[Mo_3S_{13}]^{2-}$ cluster anion on the surface of γ-Al_2O_3 as derived from the IET spectrum.

$\nu(Mo-S)_{br}$ = 387 (*vs*), 354 (*s*); $\nu(Mo-S)_t$ = 332 (*m*), 298 (*m*) cm^{-1} and is also compatible with electrostatic considerations.

From quantum chemical calculations (26) we know that the terminal S_2 groups have a significantly higher negative charge than the bridging ones. This can also be rationalized from their chemical behavior: the bridging S_2 entities are selectively attacked by nucleophilic and, correspondingly, the terminal ones by electrophilic (oxidizing) agents (36). For this reason the terminal S_2 groups are preferred for contacts with the positively polarized [110] surface of Al_2O_3 (37) which is believed to form the most stable surface plane of alumina (38). These interfacing terminal S_2 groups should show a shift of the corresponding $\nu(S-S)_t$ frequency to lower wavenumbers. However, because the S–S vector is normal to the tunneling direction there is no contribution by them to the observed intensities. It is interesting to note that we found a completely analogous orientation of the anion prepared on graphite layers in a scanning tunneling microscope (STM) study (39).

The $(NH_4)_2[Mo_3S_{13}] \cdot H_2O$ cluster compound decomposes upon heating to MoS_2 type crystallites (4):

$$(NH_4)_2[Mo_3S_{13}] \cdot H_2O \rightarrow 2NH_3 + H_2S + 3MoS_2 + 6S^0 + H_2O$$

After the loss of the apical μ_3 sulfur atom and the further loss of neutral sulfur, the $\{Mo_3S_x\}$ triangles condense to larger units without a redox reaction at the Mo(IV) centers at temperatures above 580 K (4, 5). A perfectly stacked MoS_2 lattice, however, is only reached at much higher temperatures (19, 40).

Figure 5 shows the infrared emission spectrum of crystalline MoS_2, i.e., two major bands at 461 and 376 cm^{-1} (corresponding to the room temperature values for the $\nu(A_{2u})$ and $\nu(E_{1u})$ vibrations at 466 and 384 cm^{-1} (41), respectively) and some weak features between 500 and 560 cm^{-1} (due to ν(S–S) vibrations of different kinds of coordinated S_2 groups). The spectrum of microcrystalline MoS_2 (as prepared from MoO_3 by sulfidation, Fig. 5a) shows distinct bands with medium intensity in the latter region (555, 542, 531, and 509 cm^{-1}). It is interesting to note that the intensity of these signals decreases when the sample is kept in a flow of pure argon at 670 K for 1 h (Fig. 5b) and becomes zero when pure hydrogen is used instead of argon. This observation is important and will be discussed below. In both cases the initial spectrum can be nearly restored by resulfidation in an H_2S/H_2 atmosphere.

The vibrational spectra of the final decomposition product of the cluster compound are shown in Fig. 6 (IRE (a), Raman (b), and IET (c); b and c on alumina). They are clearly related to those of MoS_2 with bands at 464 and 380 cm^{-1} (IRE, $\nu(A_{2u})$ and $\nu(E_{1u})$, see above) and at 410 and 376 cm^{-1} (Raman, $\nu(A_{1g})$ and $\nu(E^1_{2g})$ (41). An important aspect is that the half-width of the bands in the Raman spectrum can be correlated with the average particle size (8). For microcrystalline MoS_2, as obtained from the thermal decomposition of $(NH_4)_2[Mo_3S_{13}] \cdot H_2O$, a diameter around 5500 pm and an average stacking of more than 3 slabs per crystallite was found in the HREM (6).

Figure 6a shows also signals at 531 cm^{-1} (cf. Fig. 5a) and at 408 cm^{-1}, corresponding to the (in principle) only Raman active $\nu(A_{1g})$ type vibration. We therefore conclude that a sufficient number of edge molybdenum atoms must be present in an environment which differs from the ideal trigonal prismatic coordination dominating in the bulk MoS_2 structure, and that the selection rules no longer apply strictly (note that formally the selection rules for solid state vibrational spectroscopy are in force only for an infinite number of atoms (42)). Corresponding phonon signals of MoS_2 in the IET spectrum (Fig. 6c) are found at 460 (*m*), ($\nu(A_{2u})$); 411 (*m*), ($\nu(A_{1g})$); 379 (*m*), ($\nu(E_{1u})$ or $\nu(E^1_{2g})$) and 289 cm^{-1} (*vs*), ($\nu(E_{1g})$). Two additional and quite strong bands, i.e., a broad one at 830 and another at 243 cm^{-1} should then be related to the type of interaction of the MoS_2 crystallites with alumina (Mo–O–Al bridges). IET turns out to be particularly sensitive to this kind of linkages which are not "seen" by other techniques, such as EXAFS, probably due to their low abun-

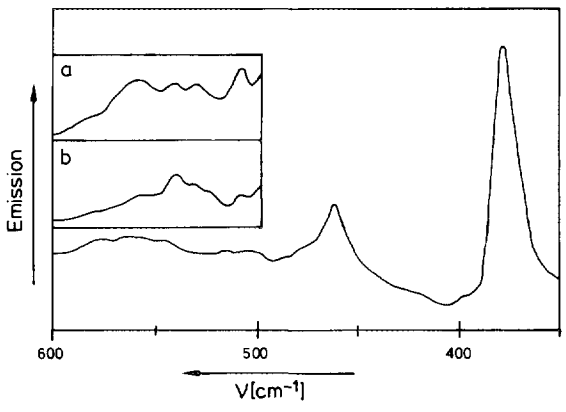

FIG. 5. IRE spectrum of 2H-MoS_2. Section (a) shows the IRE spectrum of microcrystalline MoS_2 obtained from MoO_3 directly after sulfidation and section (b) the same after keeping the sample for 1 h in Ar atmosphere.

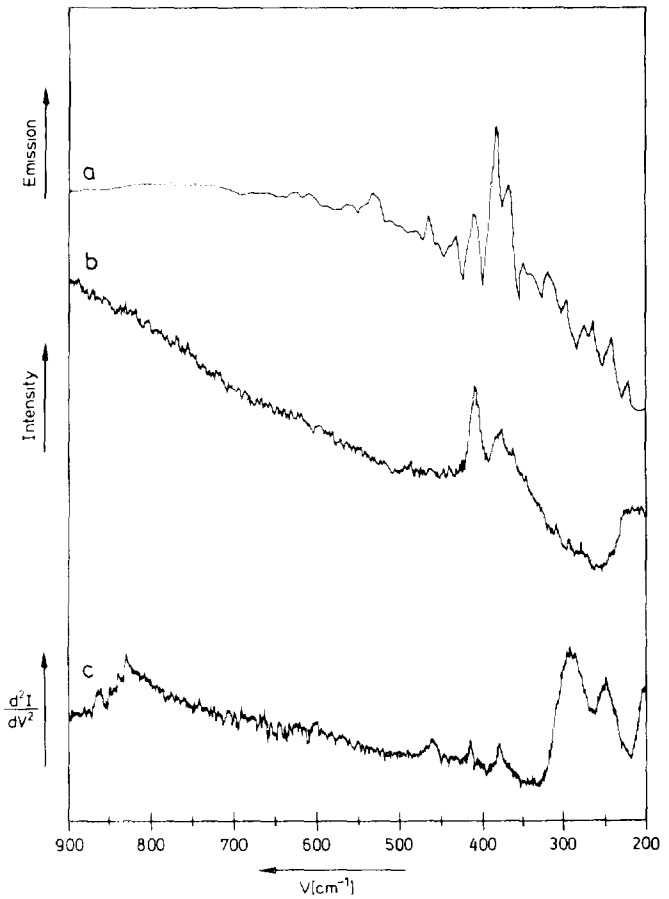

FIG. 6. IRE (a), Raman (b), and IET (c) spectra of MoS_2 as obtained from the thermal decomposition of $(NH_4)_2[Mo_3S_{13}] \cdot H_2O$ ((a) without support; (b) and (c) on γ-Al_2O_3).

dance. We assign these two bands to the ν_{as}(Mo–O(–Al)) and ν_s(Mo–O(–Al)) vibrations of the corresponding linkages, respectively. These findings will allow us to determine the orientation of the MoS_2 crystallites relative to the [110] surface of γ-Al_2O_3.

The vibrations of MoS_2 can be separated into two kinds of normal modes, those parallel to the c-axis (A_{2u}, A_{1g}) and those parallel to the basal planes of the crystallites (E_{1u}, E^1_{2g}, E_{1g}) (43). With either a parallel or perpendicular orientation of the slabs on the alumina support, definitely different spectral features are to be expected in the IET spectrum, i.e. high intensities of the "c-axis mode" signals, in the case of a parallel orientation or, reversely high intensities of the "basal-plane mode" signals for a perpendicular arrangement. The spectroscopic result (Fig. 6c) implies a situation somewhere in between where *the orientation of the slabs is more close to the perpendicular orientation*. This follows from the observed intensities but it is also implied by the values and the difference between the frequencies of the ν_s(Mo–O(–Al)) and ν_{as}(Mo–O(–Al)) vibrations. For M–O–M bridges (as a simple model for the heteronuclear M–O–M' system) this can be roughly estimated from the equations given by Cotton and Wing (44):

$$\lambda_s = [\mu_M + \mu_O(1 + \cos\varphi)](k + k_i)$$
$$\lambda_{as} = [\mu_M + \mu_O(1 - \cos\varphi)](k - k_i)$$

($\lambda = 5.889 \cdot 10^{-7} \cdot \nu^2$, where ν^2 is the square of the wavenumber (in cm^{-1}) and μ_M as well as μ_O are reciprocals of the masses of the metal and the oxygen atom, respectively (in a.m.u.$^{-1}$); φ is the angle of the M–O–M bridge; k and k_i give the stretching force constant and the stretch-stretch interaction force constant in mdyn/Å, respectively). From these equations it is obvious that the difference between the symmetric and antisymmetric vibrational frequencies for given force constants depends strongly on the angle φ. Furthermore, the antisymmetric M–O–M stretching vibration should have a much higher frequency than the symmetric one in both the linear and the bent systems, since in the latter almost only the (light) oxygen atom is vibrating between the two metal atoms with much higher masses.

A corresponding result is also obtained for the more realistic model of a triatomic X–Y–Z type system. Assuming approximately vanishing interactions between the bending vibrations and the two stretching vibrations, it is easy to show from the G matrix elements (45) for the stretching vibrations ($G_{11} = \mu_X + \mu_Y$, $G_{12} = \mu_Y \cdot \cos\varphi$, $G_{22} = \mu_Z + \mu_y$) that the coupling between them (stronger coupling means larger frequency difference) increases with an increasing φ and a decreasing mass of the central atom Y.

To obtain an estimate for the actual values of φ and the Mo–O distance of our system we compare the data with those of the $[O_3Mo–O–MoO_3]^{2-}$ anion (ν_s(Mo–O) = 201 cm^{-1}, ν_{as}(Mo–O) = 835 cm^{-1}) (46) where φ = 153.6° and $d(Mo–O)_{br}$ = 187.6 pm (47). In the case of the $[O_3Cr–O–CrO_3]^{2-}$ anion we have, e.g., a much smaller frequency difference: ν_{as}(Cr–O) = 776, ν_s(Cr–O) = 557 cm^{-1} (48), and, correspondingly, φ = 121° (49). Therefore, the Mo–O–Al bond angle is expected to be significantly higher than 120° but lower than 150° and probably very close to the latter. Taking φ = 140° and using the above given frequencies and equations we obtain a slightly larger Mo–O stretching force constant for our system than for the Mo–O–Mo bridge in the $Mo_2O_7^{2-}$ anion. We therefore conclude that there is a slightly shorter Mo–O distance, namely 185 pm. This value however, is only the average of a distribution of distances since the half-width

of the corresponding signal is significantly higher than expected by temperature broadening alone. Taking the observed half-width we find an actual range from 132° to 145° for the Mo–O–Al angle.

We then tried to verify the situation by molecular modeling calculations. γ-Al_2O_3 has a defective spinel structure where the oxygen atoms form an almost perfect cubic-closed packing and the Al^{3+} centers fill octahedral and tetrahedral holes. The unit cell dimension ($a_0 \approx 820$ pm) is determined primarily by the close-packing of the oxygen atoms. The [110] plane which only consists of closed-packed O^{2-} anions in alternating rows was generated for the modeling calculations as a fixed substructure according to known X-ray data (50). First we modeled the situation as envisaged by Hayden and Dumesic (51) (Fig. 7), with a perpendicular arrangement of the layer's [$2\bar{1}\bar{1}0$] face to the support (by spreading the interfacing sulfur atoms of the MoS_2 out of their original positions and docking each Mo atom to every second O atom of the alumina plane). The crystallite is then track-like fixed on the upstanding row of the slab. Also the inclusion of further slabs with the correct stacking and a proper binding to the support is not possible. We have then tried another, probably more realistic, arrangement which is displayed in Fig. 8. The MoS_2 slabs are adjusted via their [$1\bar{1}00$] edges on two directly neighboring upstanding oxygen rows. We obtain a relatively stress-free arrangement if each Mo atom is bonded to every second oxygen atom associated with tetrahedrally coordinated Al with an Mo–O distance of 185 pm as indicated schematically in Fig. 8. For a single layer there is only a minor energy change when the Mo–O–Al angle varies. With more than one layer bound in the described way to the next oxygen rows we obtained a significant inclination of the whole assembly. Due to the slightly different spacings of the oxygen and molybdenum atoms within and between the corresponding layers, the formation of the Mo–O bonds causes some distortion in the MoS_2 crystallites, producing

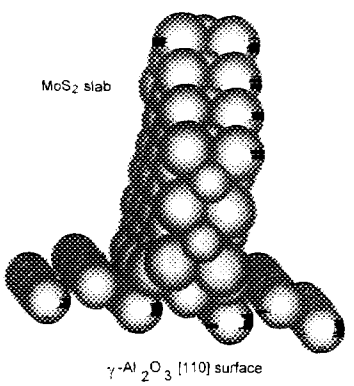

FIG. 7. Adjustment of an MoS_2 crystallite via is [$2\bar{1}\bar{1}0$] face on the [110] surface of γ-Al_2O_3 according to Ref. (51) as obtained from the molecular modeling calculations.

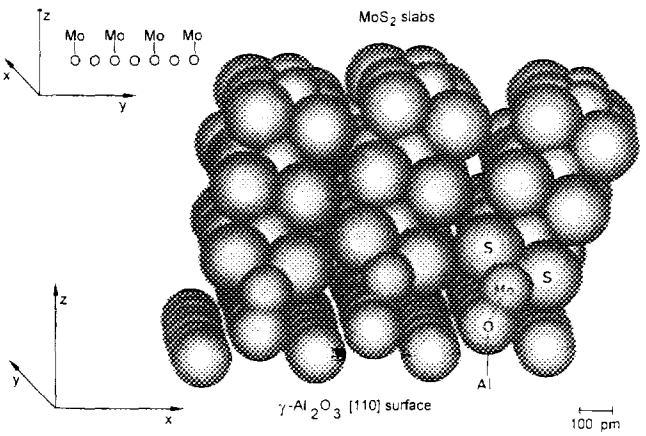

FIG. 8. Adjustment of three MoS_2 crystallites via their [$1\bar{1}00$] planes on the [110] surface of γ-Al_2O_3 as obtained from the molecular modeling calculations.

a fan-like structure in the stacking of the layers. However, this is probably of less importance for the real crystallites because they are much larger as shown in Fig. 8 and the forces required to distort such a unit will also be much higher. If the Al atoms are assumed fixed at crystallographically adequate positions, *modeling yields a range for the Mo–O–Al bonding angle from 135° to 148° which neatly matches the above given estimate from our IETS results.*

We now comment on the surface structure of the catalyst crystallites themselves and the role of hydrogen within the catalytic cycle. Unfortunately, Al_2O_3 is a strong absorber in the infrared region, and therefore only "unsupported" samples could be studied using infrared emission spectroscopy. The IRE spectra (Fig. 5) clearly show that S_2 groups[1] are present on the surface of the MoS_2 particles at 670 K, even in the case of the macrocrystalline 2H–MoS_2. From the related chemistry of disulfur complexes we have knowledge of an overwhelming variety of possible structures (52). According to our classification of the different S_2 coordination types (52, 53), two of them are relevant to our problem, i.e., type Ia (side-on) and type III. In the latter both sulfur atoms are bonded to two metal atoms, with the S–S bond orientated nearly normal to the metal–metal vector:

type I a type III

Note that both kinds of coordination of the S_2 ligand are present in the $[Mo_3S_{13}]^{2-}$ cluster anion. Bands due to ν(S–S) vibrations of both types of coordination are ob-

[1] This is a formal description, as the real charge of the S_2 ligands may vary between 0 and 2− but is usually found nearer to 2−.

served in the IR. Vibrational bands related to type III are generally observed at higher wavenumbers (≈540–550 cm^{-1}) than those of the Ia type structure (≈510 cm^{-1}).

Upon heating in an inert gas atmosphere, type Ia S_2 groups are typically released even at quite low temperatures due to a reductive elimination reaction (4, 5, 54). (e.g., from $Cs_2[(S_2)_2Mo(S_2)_2Mo(S_2)_2]$ free gaseous S_2 can be generated even at temperatures below 470 K (52)).

$$\{Mo^n\}\text{–}(S_2^{2-}) \rightarrow \{Mo^{n-2}\} + S_2$$

This causes a decrease in the intensities of the S_2 bands in the spectrum in Fig. 5b, compared to those in Fig. 5a, and is accompanied by the generation of reduced Mo centers ($Mo^{IV} \rightarrow Mo^{II}$) on the surface of the crystallites. If this occurs at (only) one Mo center there is the possibility of the formation of a type III substructure from which S_2 can only be removed at much higher temperatures. It will therefore lead to a blocking of the involved Mo atoms for substrate adsorption as shown in reaction Scheme I.

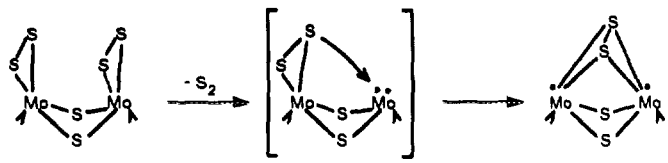

SCHEME I

However, if H_2 is applied to such a system also the bridging S_2 groups can be mobilized (55) yielding a further reduced and strongly coordinatively unsaturated ("activated") surface of the crystallites as shown formally in Scheme II. Metal-to-metal interactions and/or an electron delocalization of the type $Mo^{II} \rightarrow (Mo^{IV})_n$ have to be considered for the stabilization effect on the transition state.

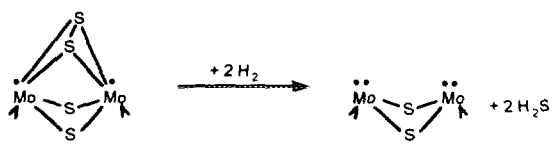

SCHEME II

This pretreatment with hydrogen turns out to be an essential prerequisite for the coordination of substrates to the catalyst surface. In order to obtain vibrational spectra of thiophene chemisorbed on the MoS_2 surface with the *in situ* Raman and IRE technique, we first tried to load the only thermally pretreated catalysts with the substrate in an argon stream. In this case spectra of a lower degree of complexity were expected because H_2 as the main HDS reactant was absent. However, all of these experiments failed and *spectra showing bands related to chemisorbed thiophene could only be obtained when hydrogen was used instead of argon*. To check the conditions for the thiophene chemisorption with an additional independent experiment we performed some TPD measurements on this system.

Figure 9 shows the TPD profiles of the MoS_2/Al_2O_3 catalysts loaded with thiophene in a hydrogen (a) and argon stream (b) and of alumina without catalyst (c). Desorption of coked materials, beginning at approximately 670 K, is a common property of all samples investigated, but signals related to thiophene desorption are only found in the case of sample (a): these are three weak (480, 510, and 640 K) desorptions and one major (580 K) desorption. After "ageing" this sample for some time, the different features due to thiophene desorption are replaced by only one broad signal at ≈530 K. The presence of one broad desorption band corresponds to a distribution of desorption energies and might be explained in terms of the surface structure of the crystallites including also less favourable coordination geometries (see below). Thiophene adsorption on this type of catalyst then occurs at essentially one type of coordination site only in the presence of hydrogen. The results clearly show that *hydrogen is not only a reactant within the HDS reaction but also of fundamental importance in making the catalyst susceptible for substrate chemisorption.*

The different vibrational spectra of thiophene chemisorbed on the surface of the MoS_2 crystallites are displayed in Fig. 10 and compiled in Table 1. In addition, bands at 518 (ν(S–S) (residual S_2 groups)), 397 ($\nu(A_{1g})$), 365 ($\nu(E^1_{2g})$ characteristic for MoS_2) and 262 cm^{-1} are present in the Raman spectrum (Fig. 9b). The shift of the $\nu(A_{1g})$ type vibration (15 cm^{-1}) to lower wavenumbers compared to crystalline MoS_2 (8) is caused by hydrogen intercalation between the MoS_2 layers (56). This intercalation is probably of great importance for the catalytic turn-

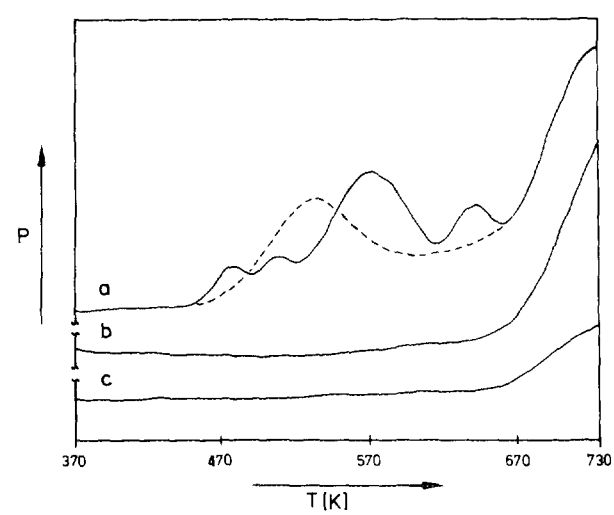

FIG. 9. Temperature programmed desorption profiles of the MoS_2/Al_2O_3 catalyst loaded with H_2/thiophene (a) and Ar/thiophene (b) and of pure γ-Al_2O_3 treated as (a). The broken line in (a) indicates the behaviour after ageing (see text).

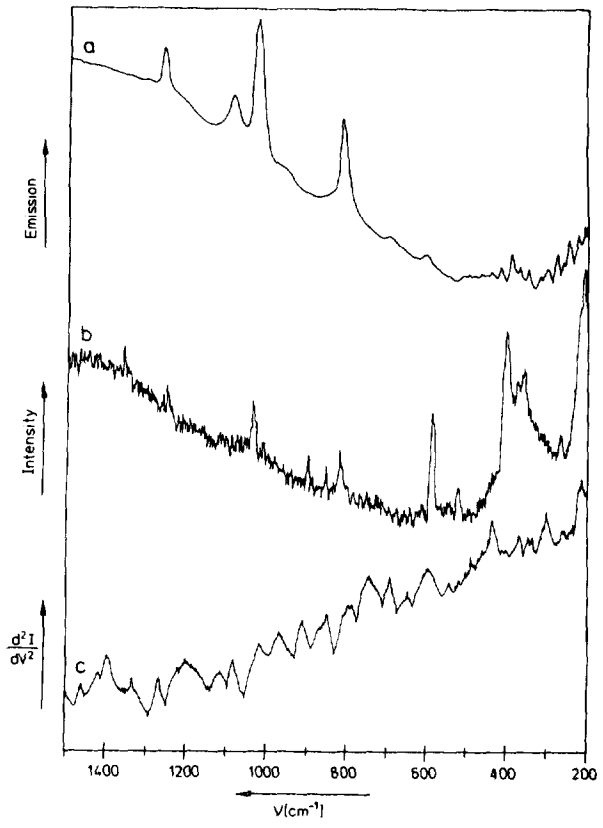

FIG. 10. IRE (a), Raman (b), and IET (c) spectra of adsorbed thiophene ((a) without support; (b) and (c) on γ-Al_2O_3).

over since hydrogen is preconcentrated near the active sites (cf., e.g., Delmon in Ref (2)). Furthermore, we see a couple of signals in the IET spectrum which do not correspond directly to chemisorbed thiophene but may be already due to reaction products. Recall that the history of the preparation of this tunnel junction is not exactly the same as the sample preparation for the Raman and IRE probes. Even a small amount of hydrogenation and, primarily, coking products which may be fairly quenched in the IET probe clearly contribute to the obtained spectra if they have a proper orientation relative to the tunneling direction.

It is evident from Table 1 that those bands mainly due to ν(C–H), δ(C–H) and $\nu(C_2–C_3)$ type vibrations show no large shift upon coordination, i.e., the bands at 1358(Raman), 1266(IRE), 1260(IET), 1084(IRE), 1083(IET), 1031(IRE), 1033(Raman), 1030(IET), and 899(IET) cm^{-1}. Others at 817(IRE), 815(Raman), 693(IRE, IET), 585(Raman), 597(IET) and 436(IET) cm^{-1} show shifts between 8 and 23 cm^{-1} to lower wavenumbers. The corresponding not very characteristic vibrations depend significantly on the contributions of the C–S and C=C stretching coordinates. Therefore, every theoretical model for thiophene coordination must also explain the destabilization of the C–S and C=C bonds of this substrate.

To obtain an impression of the spatial requirements for a substrate coordination we have again used computer modeling and attached a thiophene molecule with its sulfur atom to a free edge Mo atom (corresponding to a situation after treating the sample with hydrogen as indicated in reaction Scheme II). As a typical result, Fig. 11 shows two thiophene molecules attached as flat as possible to two neighboured Mo sites of one MoS_2 slab. If this edge of the crystallite forms the real top of the assembly there is much freedom for a thiophene molecule and also for larger substrates like dibenzothiophene to be

TABLE 1

Selected Bands (in cm^{-1}) of Free (Liquid) and Coordinated Thiophene in the IR, Raman, and IET Spectrum and Their Assignments According to Ref. (72)

IRES coordinated	IR free	displacement vectors	Raman free	Raman coordinated	IETS coordinated
			1362	1358	
1266	1261 (1262)				1260
1084	1081 (1081)				1083
1031	1034 (1035)		1036	1033	1030
			905	897	899
817	835 (838)		836	815	
693	715 (712)				693
			608	585	597
	452 (452)		455		436

Note. The values in parenthesis are those of gaseous thiophene at 670 K.

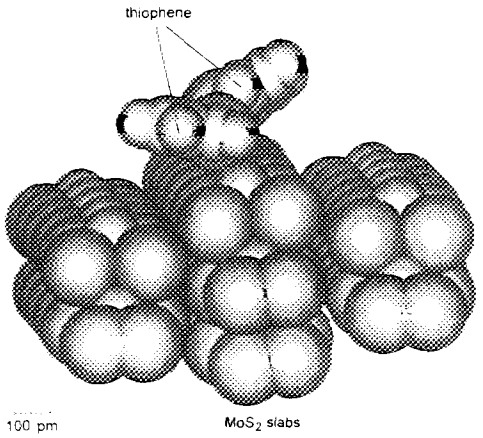

FIG. 11. Docking of two thiophene molecules to "free" Mo sites on the "edge" surface of an MoS_2 particle consisting of three slabs as obtained from the molecular modeling calculations.

coordinated (as depicted in Fig. 12). *However, if the active sites are not at the top but below (e.g., between two layers), it becomes difficult for large substrates to attach properly due to steric hindrance by the atoms of neighbouring slabs.* Here we see a major reason for the fact that large substrates are in general less susceptible to the HDS reaction.

What is now the reason for the coordination of thiophene and other sulfur-containing ligands at all? Molecules of the type RSH and RSR are "poor" ligands (53, 57) but thiophene is obviously even less suited for complex formation. Two kinds of coordination of thiophene to metal centers have been detected so far, namely bonding via the sulfur atom alone (to give an *M*–S–C angle considerably less than 180°) or a *hapto* arrangement of the ring (η coordination) (58). In the latter case all four metal-to-carbon distances are almost the same and, typically, the metal-to-sulfur distance is slightly larger than expected for *M*–S single bonds. This situation is found in many organometallic complexes. However, we do not favour this kind of coordination in our catalyst because this would increase the probability of retaining *M*–C bonds during the reaction. Coking of the site or an increased formation of C_1, C_2, and C_3 species then consequently should be observed. Both events are obviously not of major importance. Coking, for example, happens in practice as an inhibiting process but is only a long term problem.

We observe a strong signal in the IET spectrum (Fig. 10c) at 300 cm^{-1}. This band should be assigned to a ν(Mo–S) vibration as the wavenumber corresponds to the range expected for vibrations of species with *M*–S single bonds, a situation which clearly favours the abundance of an S-bonded thiophene, although an unequivocal decision based on the obtained vibrational results cannot be made. We exclude a complete perpendicular coordination of the S-bonded thiophene for theoretical reasons. Also a considerable steric effect would be expected here upon substitution with bulky groups in the 2,5 position and consequently a hindrance for the HDS reaction. The reverse has been found experimentally, e.g., 2,5-dimethylthiophene shows a better HDS susceptibility than thiophene (59).

Only very few and not well characterized S-bonded thiophene complexes with low-valent metal centers have been reported (58) and, in fact, we also could not find any complex formation with our thermally pretreated catalyst. Only after considerably increasing the basicity of the Mo centers by further reduction with hydrogen did a coordination occur. This seems very similar to the behaviour of the dinitrogen molecule, which is also a "poor" ligand but shows coordination when the metal centers are reduced, e.g., from Ru^{III} to Ru^{II} (60) or from Fe^{III} to Fe^{II} (61). Here, the delocalization of the increased number of d electrons from the reduced centers into low-lying antibonding levels of the ligand makes the coordination favourable. We assume a corresponding situation for the coordination of thiophene, where it would not make too much difference whether it is S- or η-bonded. Figure 13 shows the HOMO/LUMO region of free thiophene as obtained from our EH-MO calculations. While the highest occupied level is π (C=C) bonding in character, a population of the first LUMO's should result primarily in a destabilization of the C=C and C–S bonds, just as in inferred from our spectral data for the coordinated thiophene.

To obtain at least a qualitative picture of the electronic structure of the reduced Mo centers on the catalyst we have made EH-MO calculations for a hypothetical situation which derives from our precursor anion. For the purpose of simplification only three metal atoms are involved. We started with a calculation for an $[Mo_3S_{13}]^{2-}$ ion for which one terminal S_2 group had been removed, i.e. for a (hypothetical) $[Mo_3S_{11}]^{2-}$ ion. We took the interatomic distances from the data of the X-ray structure

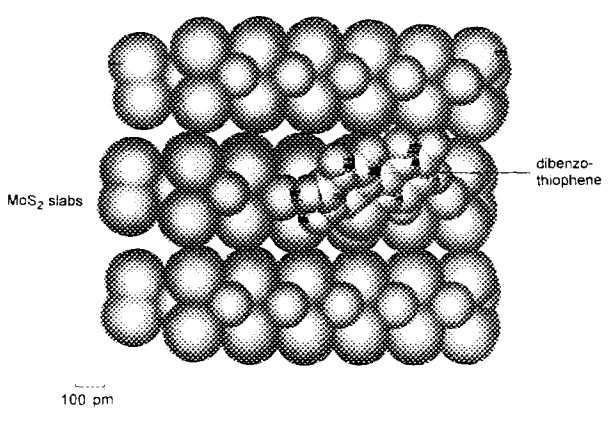

FIG. 12. Coordination of a dibenzothiophene molecule to a free Mo site on the "edge" surface of an MoS_2 particle consisting of three slabs as obtained from the molecular modeling calculations.

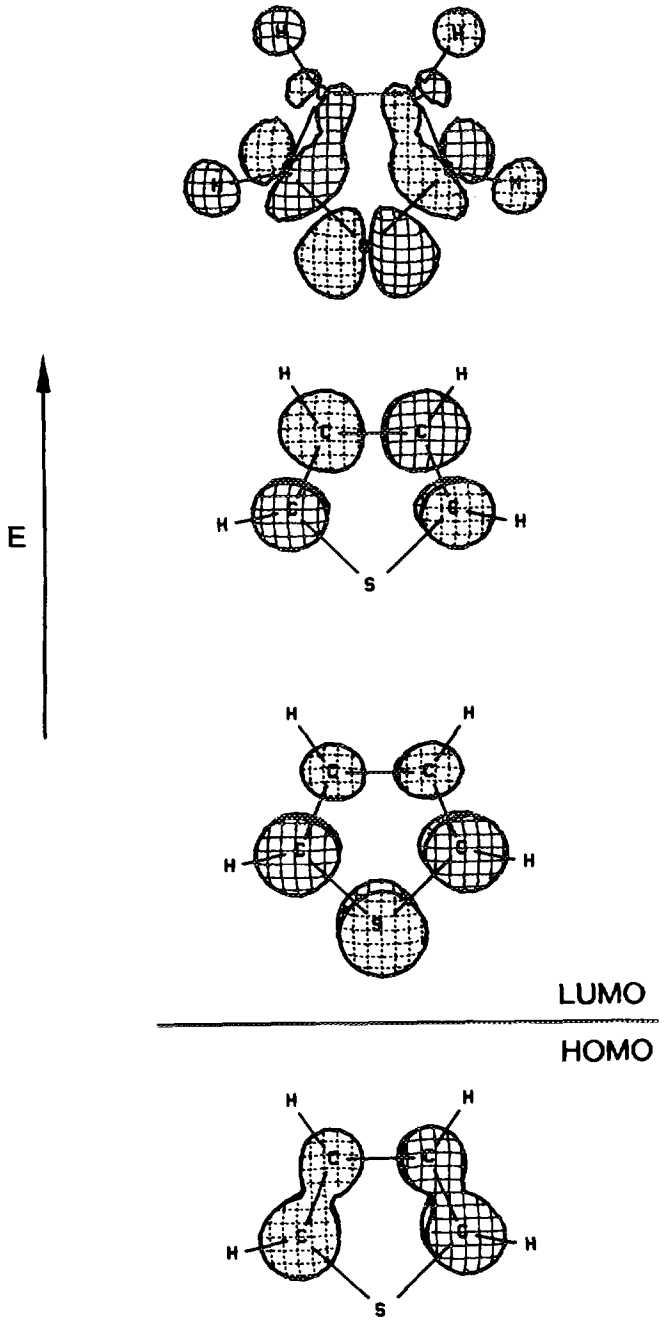

FIG. 13. Orbital plots of thiophene in the HOMO/LUMO region.

of $(NH_4)_2[Mo_3S_{13}]$, e.g., the Mo–Mo distances of 272 pm. These are, of course, much shorter than the Mo–Mo distances of 315 pm in bulk crystalline MoS_2, but this assumption is not unreasonable in view of the presence of reduced $Mo^{(II)}$ centers allowing Mo–Mo interactions at the surface of the crystallites. There are two metal atom neighbours in the case of the $[Mo_3S_{11}]^{2-}$ ion compared to six in MoS_2 (cf. also our discussion in Ref. (5) and the experimental results of Agostini *et al.* (62) who found by EXAFS a considerable decrease of the average Mo–Mo distance in MoS_2 particles with decreasing size). The most interesting result of our calculation is the obtained charge distribution in this hypothetical anion. The metal atoms still carry a slightly positive charge and the coordinatively unsaturated Mo atom is the less positive one. The negative charge, however, is completely located on the sulfur atoms which seem to act as an electron sink (cf. also Ref. (63)).

Next, we modeled an S-bonded thiophene to this free site, keeping the $[Mo_3S_{11}]^{2-}$ unit as a fixed structure. Modeling yielded here completely analogous results of *M*–S–C distances and angles to those recently found experimentally by Angelici *et al.* (64) for 2,5-dihydrothiophene complexes of ruthenium. The EH-MO result for the HOMO of our model complex taking the coordinates for the docked thiophene as obtained from the force field energy minimization is displayed in Fig. 14. It clearly shows that *now the electron density from the "reduced" metal cluster ion is delocalized into the first antibonding level of thiophene* and thus, as already verified by our experiments, destabilizes the C–S and C=C bonds of this ligand, making it susceptible for further reaction with hydrogen. This confirms the conclusions of Zonnevylle *et al.* (65) although they assumed a rather short Mo–S distance of 190 pm (which would correspond to multiple bonding) for their calculations.

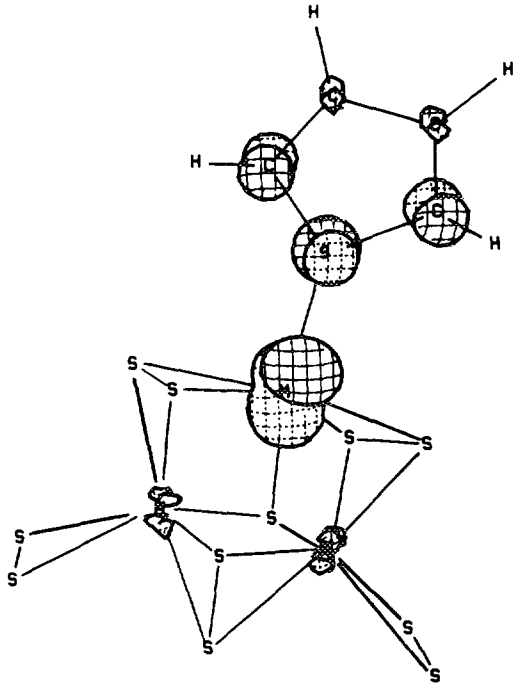

FIG. 14. Highest occupied molecular orbital of a hypothetical complex formed by coordination of a thiophene ligand to the unsaturated Mo site of an $[Mo_3S_{13}]^{2-}$ cluster anion where a terminal S_2 group has been reductively eliminated, i.e., yielding an $[Mo_3S_{11}]^{2-}$ ion.

The results from the MO calculations apply, in principle, also to other sulfur-containing molecules present in crude oils, e.g. RSH, RSR, and R_2CS type species. Because the valence state ionization energy (VSIE) of S 3*p* has one of the highest values in the assembly and the local symmetry of sulfur in the coordinated case is intrinsically low, this level will *always* be involved strongly in the orbitals of the HOMO/LUMO region. Any population of the antibodingorbital will then lead also to a destabilization of the C–S bond. In practice hydrogenation of such compounds can be achieved with the SCOT process (Shell Claus off gas treatment) using Co–Mo catalysts under much less demanding conditions than required for the HDS reaction (66).

We were not concerned with the next steps of the reaction mechanism in detail but in fact it could follow the route of a Birch reduction (67) which is a well-known reaction mechanism in organic chemistry and has already been discussed in this regard by Prins *et al.* (1). According to the successive transfer of electrons and protons (which are obtained in the original reaction from a solution of alkali metals in liquid ammonia in presence of methanol) aromatic compounds are reduced, i.e. in the case of thiophene 2,3-dihydro- and 2,5-dihydrothiophene occur as the first reduction products. These compounds might also be relevant intermediates during the HDS reaction where in a later step of the reduction hydrogen atoms are transferred from β-positions to the thiophene sulfur atom while breaking the C–S bond. (This would be in line with the results of the H/D isotope substitution experiments reported by McCarty and Schrader (68).) The protons required for the Birch reduction may be generated from the intercalated hydrogen. Hydrogen-loaded MoS_2 samples of the form H_xMoS_2 ($x = 0.1 - 0.8$) were found to behave like Brønsted acids (69) where H_2 may dissociate upon intercalation yielding H^+ ions and electrons (cf. also Ref. (70)). These populate (within the "rigid band model") the conduction band and will further increase the basicity of the MoS_2 layers (vide supra).

The reaction cycle may end with the cleavage of the C–S bond giving a reduced hydrocarbon, which would be clearly butadiene when starting with thiophene, and an H_2S ligand remaining at the low-valent Mo site. Complexes of hydrogen sulfide are known to be rather unstable, particularly at higher temperatures (53). The thermal decomposition will immediately release H_2S and restore the reduced Mo site to that which it was at the beginning of the catalytic cycle. The hydrocarbon, i.e., butadiene, may then undergo further hydrogenation reactions at another site.

Gachet *et al.* (71) have studied the hydrodesulfurization of dibenzothiophene using a ^{35}S labelled catalyst surface and observed $H_2{}^{35}S$ in the reaction atmosphere. Their main conclusion from this observation was that a "turnover" between surface sulfur atoms and the sulfur atoms eliminated from dibenzothiophene should occur. However, since this experiment was done in a batch reactor and no information on the time dependence of the release of $H_2{}^{35}S$ could thus be obtained, we do not know whether the labelled product originates from the activation step (vide supra) alone or whether an exchange with the sulfur atoms of the substrate molecule was already involved. We argue here that no such exchange has to be involved to explain the experimental findings. Suffice to say here that our mechanistic view of the HDS reaction has (apart from the initial coordination step) some correspondence to the cycle proposed by Angelici *et al.* (64) which has been derived from the reactions of related organometallic compounds.

CONCLUSIONS

The results of our *in situ* Raman, infrared emission, and inelastic electron tunneling spectra accompanied by thermal desorption studies, molecular modeling and Extended Hückel MO calculations on our experimental model catalyst, i.e., MoS_2 crystallites on a γ-Al_2O_3 support as obtained from the thermal decomposition of $(NH_4)_2[Mo_3S_{13}] \cdot H_2O$, may be interpreted as follows.

(i) The catalyst consists of MoS_2 crystallites which are considerably larger than assumed for some special cases (1, 2). Their average diameter is around 5500 pm and they contain more than 3 slabs.

(ii) The slabs of the crystallites are oriented almost perpendicular to the surface of the support at temperatures relevant to the HDS reaction, slightly inclined to give an Mo–O–Al connection with a distribution of single bond Mo–O distances around 185 pm and Mo–O–Al angles around 140°. This is a compromise between *either* an Mo–O–Al angle as low as possible (for maximum overlap) and the maximal number of Mo–O–Al bonds formed from each slab to the support (while retaining the correct stacking) or the van der Waals repulsion between the oxygen atoms of the support and the "first" sulfur atoms of the MoS_2 slabs.

(iii) Active (formally Mo^{II}) sites for the HDS reaction are located at the top positions of the slabs and *coordination* of thiophene to these sites is *only* obtained after pretreatment with hydrogen under working conditions.

(iv) The sulfur-containing substrate molecule acts as a Lewis acid and is thereby destabilized and made susceptible for further reaction with hydrogen. This may follow the route of a Birch reduction within the first steps.

ACKNOWLEDGMENTS

Financial support by the Fonds der Chemischen Industrie and the Minister für Wissenschaft und Forschung NRW is gratefully acknowledged. We dedicate this paper to Professor Pedro J. Aymonino, in

recognition of a long period of fruitful cooperation, on the occasion of his 65th birthday.

REFERENCES

1. Prins, R., de Beer, V. H. J., and Somorjai, G. A., *Catal. Rev.-Sci. Eng.* **31,** 1 (1989), and references cited therein; Knözinger, H., "Proc. 9th Int. Congr. Catal. (Calgary, 1988)" (M. J. Phillips and M. Ternan, Eds.), Vol. 5, p. 20, The Chemical Institute of Canada, Ottawa, 1989; Müller, A., Diemann, E., and Baumann, F.-W., *Nachr. Chem. Techn. Lab.* **36,** 22 (1988).
2. (a) Delmon, B., *in* "Catalysis in Petroleum Refining" (D. L. Trimm, S. Akashah, M. Absi Halabi and A. Bishara, Eds.), p. 1. Elsevier, Amsterdam, 1990. (b) Topsøe, H., Clausen, B. S., Topsøe, N.-Y., and Zeuthen, P., *in* "Catalysis in Petroleum Refining" (D. L. Trimm, S. Akashah, M. Absi Halabi and A. Bishara, Eds.); p. 77. Elsevier, Amsterdam 1990. (c) See also "Proc. IVth Workshop on Hydrotreatment," *Bull. Soc. Chim. Belg.* **100,** 769–991 (1991).
3. Müller, A., Diemann, E., Krickemeyer, E., Walberg, H.-J., Bögge, H., and Armatage, A., *Eur. J. Solid State Inorg. Chem.* **30,** 565 (1993).
4. Diemann, E., Müller, A., and Aymonino, P. J., *Z. Anorg. Allg. Chem.* **479,** 191 (1981).
5. Müller, A., and Diemann, E., *Chimia* **39,** 312 (1985).
6. Müller, A., Diemann, E., Branding, A., Baumann, F. W., Breysse, M., Vrinat, M., *Appl. Catal.* **62,** L13 (1990).
7. Dixit, L., Gerrard, D. H., and Bowley, H. J., *Appl. Spectrosc. Rev.* **22,** 189 (1986).
8. Müller, A., and Weber, Th., *Appl. Catal.* **77,** 243 (1991).
9. Griffiths, P. R., *Appl. Spectrosc.* **26,** 73 (1972); Van Woerkom, P. C. M., and De Groot, R. L., *Appl. Opt.* **21,** 3114 (1982); Nagasawa, Y., and Ishitani, A., *Appl. Spectrosc.* **38,** 68 (1984).
10. Wolfram, T., (Ed.), "Inelastic Electron Tunneling Spectroscopy," Proc. Int. Conf. Symp. Electron Tunneling, Univ. Missouri-Columbia, 1977, Springer, Berlin 1978.
11. Walmsley, D. G., and Tomlin, J. L., *Prog. Surf. Sci.* **18,** 247 (1985).
12. Weinberg, W. H. (p. 359), and Kroeker, R. M. (p. 393), *in* "Tunneling Spectroscopy—Capabilities, Applications, and New Techniques" (P. K. Hansma, Ed.), Plenum, New York 1982.
13. Dawson, P. T., and Walker, P. C., *in* "Experimental Methods in Catalytic Research," Vol. III, Characterization of Surface and Adsorbed Species (R. B. Anderson and P. T. Dawson, Eds.), p. 211. Academic Press, New York, 1976.
14. Müller, A., and Krickemeyer, E., *Inorg. Synth.* **27,** 47 (1990).
15. Van Arkel, A. E., *Rec. Trav. Chim.* **45,** 442 (1926).
16. Bates, J. B., *in* "Fourier Transform Infrared Spectroscopy-Application To Chemical Systems" (J. R. Ferraro and L. J. Basile, Eds.), Vol. 1, p. 99. Academic Press, New York, 1978.
17. Barr, J. K., *Infrared Phys.* **9,** 97 (1969).
18. Jonson, B., Rebenstorf, B., Larsson, R., and Primet, M., *Appl. Spectrosc.* **40,** 798 (1986).
19. Fabbri, G., and Baraldi, P., *Appl. Spectrosc.* **26,** 593 (1972).
20. Brown, N. M. D., *in* "Spectroscopy of Surfaces" (R. J. H. Clark and R. E. Hester, Eds.), Vol. 16, p. 215. Wiley, New York, 1988.
21. Walmsley, D. G., McMorris, I. W. N., Timms, W. E., Nelson, W. J., Tomlin, J. L., and Griffin, T. J., *J. Phys. E* **16,** 1052 (1983).
22. Tomlin, J. L., *Prog. Surf. Sci.* **31,** 131 (1989).
23. Hansma, P. K., in Ref. (12), p. 1.
24. Drew, M. G. B., Mitchell, P. C. H., and Kasztelan, S., *J. Chem. Soc. Faraday Trans.* **86,** 897 (1990) and **88,** 3225 (1992); *Mol. Simul.* **9,** 143 (1992).
25. Allinger, N. L., *J. Am. Chem. Soc.* **99,** 8127 (1977); Allinger, N. L., QCPE 395 (1977); Burkert, U., and Allinger, N. L., "Molecular Mechanics," ACS Monograph No. 177, Washington, DC, 1982.
26. Müller, A., Wittneben, V., Krickemeyer, E., Bögge, H., and Lemke, M., *Z. Anorg. Allg. Chem.* **605,** 175 (1991).
27. Jostes, R., Ph.D. Thesis, University of Bielefeld, 1984.
28. Basch, H., and Gray, H. B., *Theoret. Chim. Acta* **4,** 367 (1966).
29. Clementi, E., *J. Chem. Phys.* **40,** 1944 (1964).
30. Basch, H., Viste, A., and Gray, H. B., *Theoret. Chim. Acta* **3,** 458 (1965).
31. Beach, N. A., and Gray, H. B., *J. Am. Chem. Soc.* **90,** 5713 (1968).
32. Wolfsberg, M., and Helmholz, L., *J. Chem. Phys.* **20,** 837 (1952).
33. Mealli, C., and Proserpio, D. M., *J. Chem. Educ.* **67,** 399 (1990).
34. Müller, A., Jostes, R. Jaegermann, W., and Bhattacharyya, R. G., *Inorg. Chim. Acta* **41,** 259 (1980).
35. Fedin, V. P., Kolesov, B. A., Mironov, Y. V., and Fedorov, V. Y., *Polyhedron* **8,** 2419 (1989).
36. Zimmermann, H., Hegetschweiler, K. Keller, T., Gramlich, V., Schmalle, H. W., Petter, W., and Schneider, W., *Inorg. Chem.* **30,** 4336 (1991).
37. Jimenez-Gonzales, A., and Schmeisser, D., *Surf. Sci.* **250,** 59 (1991).
38. Gates, B. C., Katzer, J. R., and Schuit, G. C. A., "Chemistry of Catalytic Processes," McGraw–Hill, New York, 1979.
39. Diemann, E., Branding, A., and Müller, A., *Bull. Soc. Chim. Belg.* **100,** 961 (1991).
40. Wildervanck, J. C., and Jellinek, F., *Z. Anorg. Allg. Chem.* **328,** 309 (1964).
41. Verble, J. L., and Wieting, T. J., *Phys. Rev. Lett.* **25,** 362 (1970).
42. Sherwood, P. M. A., "Vibrational Spectroscopy of Solids," Cambridge Univ. Press, Cambridge, 1972.
43. Wieting, T. J., and Verble, J. L., *Phys. Rev. B* **3,** 4286 (1971).
44. Cotton, F. A., and Wing, R. M., *Inorg. Chem.* **4,** 867 (1965).
45. Wilson, E. B., Decius, J. C., and Cross, P. C., "Molecular Vibrations—The Theory of Infrared and Raman Vibrational Spectra," McGraw–Hill, New York, 1955.
46. Becher, H. J., Brockmeyer, H.-J., and Prigge, U., *J. Chem. Research S* 117 (1978).
47. Day, V. W., Fredrich, M. F., Klemperer, W. G., and Shum, W., *J. Am. Chem. Soc.* **99,** 6146 (1977).
48. Weidlein, J., Müller, U., and Dehnicke, K., "Schwingungsfrequenzen II, Nebengruppenelemente," p. 69. Thieme, Stuttgart, 1986.
49. Löfgren, P., and Waltersson, K., *Acta Chem. Scand.* **25,** 35 (1971).
50. Wyckoff, R. W. G., "Crystal Structures," Vol. 3, 2nd. Ed., p. 76. Interscience, New York, 1965.
51. Hayden, T. F., and Dumesic, J. A., *J. Catal.* **103,** 366 (1987).
52. Müller, A., Jaegermann, W., and Enemark, J. H., *Coord. Chem. Rev.* **46,** 245 (1982).
53. Müller, A., and Diemann, E., *in* "Comprehensive Coordination Chemistry" (G. Wilkinson, R. D. Gillard and J. A. McCleverty, Eds.), Vol. II, Chap. 16.1. Pergamon, Oxford 1987.
54. Müller, A., *Polyhedron* **5,** 323 (1986).
55. Rakowski DuBois, M., VanDerveer, M. C., DuBois, D. L. Haltiwanger, R. C., and Miller, W. K., *J. Am. Chem. Soc.* **102,** 7456 (1980).
56. Wright, C. J., Sampson, C., Fraser, D., Moyes, R. B., Wells, P. B., and Riekel, C., *J. Chem. Soc. Faraday Trans. I* **76,** 1585 (1980); Vasudevan, S., Thomas, J. M., Wright, C. J., and Sampson, C., *J. Chem. Soc. Chem. Commun.* 418 (1982); Polz, J., Zeilinger, H., Müller, B., and Knözinger, H., *J. Catal.* **120,** 22 (1989).
57. Müller, A., and Diemann, E., *in* Ref. (53), Chap. 16.2.
58. Livingstone, S. E., *in* Ref. (53), Chapter 16.6; Angelici, R. J., *Acc. Chem. Res.* **21,** 387 (1988).
59. Choi, M.-G., and Angelici, R. J., *Inorg. Chem.* **30,** 1417 (1991).
60. Allen, A. D., and Senoff, C. V., *Chem. Commun.* 621 (1965).
61. Garcia Basallote, M., Lopez Alcala, J. M., Puerta Vizcaino, M. C., and Gonzalez Vilchez, F., *Inorg. Synth.* **24,** 207 (1986).
62. Agostini, G., Ledoux, M. J., Hilaire, L., and Maire, G., *in* "Prepara-

tion of Catalysts IV" (B. Delmon, P. Grange, P. A. Jacobs, and G. Poucelet, Eds.), p. 569. Elsevier Amsterdam, 1987.
63. Geurts, P. J. M., Gosselink, J. W., van der Avoird, A., Baerends, E. J., and Snijders, J. G., *Chem. Phys.* **46,** 133 (1980); Müller, A., Hellmann, W., Schimanski, U., Jostes, R., and Newton, W. E., *Z. Naturforsch. B* **38,** 528 (1983).
64. Choi, M.-G., Daniels, L. M., and Angelici, R. J., *Inorg. Chem.* **30,** 3647 (1991).
65. Zonnevylle, M. C., Hofmann, R., and Harris, S., *Surf. Sci.* **199,** 320 (1988).
66. (a) Bartholomé, E., Biekert, E., Hellmann, H., Ley, H., and Weigert, W. M. (Eds.) "Ullmanns Enzyklopädie der technischen Chemie," 4th Ed., Vol. 10, p. 594. Verlag Chemie, Weinheim, 1975; (b) Eastwood, S. C., Plank, C. J., and Weisz, P. B., *Proc. 8th World Petr. Congr.* **4,** 245 (1971).
67. Birch, A. J., and Nasipuri, D., *Tetrahedron* **6,** 148 (1959); see also Birch, A. J., and Subba Rao, G., *Adv. Org. Chem.* **8,** 1 (1972).
68. McCarty, K. F., and Schrader, G. L., *J. Catal.* **103,** 261 (1987).
69. Schöllhorn, R., Kümpers, M., and Plorin, D., *J. Less-Common Met.* **58,** 55 (1978); Riekel, C., Reznik, H. G., Schöllhorn, R., and Wright, C. J., *J. Chem. Phys.* **70,** 5203 (1979); Schöllhorn, R., *Physica B* **99,** 89 (1980).
70. Jessop, P. G., and Morris, R. H., *Coord. Chem. Rev.* **121,** 155 (1992).
71. Gachet, C. G., Dhainant, E., de Mourgues, L., Candy, J. P., and Fouilloux, P., *Bull. Soc. Chim. Belg.* **90,** 1279 (1981).
72. Scott, D. W., *J. Mol. Spectr.* **31,** 451 (1969).